

CdTe Quantum Dots/Layered Double Hydroxide Ultrathin Films with Multicolor Light Emission via Layer-by-Layer Assembly

Ruizheng Liang, Simin Xu, Dongpeng Yan, Wenying Shi, Rui Tian, Hong Yan, Min Wei,* David G. Evans, and Xue Duan

Quantum dots (QDs) luminescent films have broad applications in optoelectronics, solid-state light-emitting diodes (LEDs), and optical devices. This work reports the fabrication of multicolor-light-emitting ultrathin films (UTFs) with 2D architecture based on CdTe QDs and MgAl layered double hydroxide (LDH) nanosheets via the layer-by-layer deposition technique. The hybrid UTFs possess periodic layered structure, which is verified by X-ray diffraction. Tunable light emission in the red-green region is obtained by changing the particle size of QDs (CdTe-535 QDs and CdTe-635 QDs with green and red emission respectively), assembly cycle number, and sequence. Moreover, energy transfer between CdTe-535 QDs and CdTe-635 QDs occurs based on the fluorescence resonance energy transfer (FRET), which greatly enhances the fluorescence efficiency of CdTe-635 QDs. In addition, a theoretical study based on the Förster theory and molecular dynamics (MD) simulations demonstrates that CdTe QDs/LDH UTFs exhibit superior capability of energy transfer owing to the ordered dispersion of QDs in the 2D LDH matrix, which agrees well with the experimental results. Therefore, this provides a facile approach for the design and fabrication of inorganic-inorganic luminescent UTFs with largely enhanced luminescence efficiency as well as stability, which can be potentially applied in multicolor optical and optoelectronic devices.

nanocrystals.^[7] Due to the inherent advantages of QDs, they facilitate the integration of nanotechnology and biotechnology, leading to major advances in medical diagnostics, molecular biology and cell biology.^[8] From the viewpoint of optoelectronics applications, the QDs macroscopic arrays (interparticle medium, packing density and mutual orientations) impose great influence on electronic and optical communication between QDs, which to a great extent determines the behavior of QDs ensembles.^[9] Therefore, how to fabricate electronic/optoelectronic devices from QDs building blocks, including the fabrication approach, method as well as strategy, has attracted considerable attention.

Colloidal “bottom-up” synthesis and self-assembly offer the precision of size/shape engineering and placement of nanoparticles going far beyond the capabilities of current top-down lithographic techniques.^[9] Recently, incorporation of luminescent semiconductor QDs into solid matrices by self-assembly has been demonstrated to be an effective resolution

for various optical, photonic, and optoelectronic applications of quantum-confined species.^[10] The hybrid films constructed by QDs and polymers have been extensively explored so as to obtain functional composite luminescent materials and devices.^[11–15] For instance, various single color QDs films have been fabricated through LBL assembly of charged QDs with oppositely charged polymers;^[11–13] multicolor luminescence QDs films were further achieved by combining different single color QDs.^[14,15] Although the hybrid films constructed by the incorporation of QDs and organic polymers have already made much progress and corresponding devices have been developed, several problems remain unresolved. Firstly, the organic polymers tend to degrade with ultraviolet irradiation, which imposes great effects on the fluorescent properties of QDs and even leads to luminescence quenching.^[16] Secondly, thermal agitation to the polymer/QDs systems will result in changes in geometrical or electronic structure of organic species and resulting short service lifetime.^[17] Additionally, the uniformity and stacking sequence of the organic

1. Introduction

Semiconductor nanocrystals, also known as quantum dots (QDs), have received much attention over past decades in the fields of luminescent materials and optoelectronics devices.^[1,2] Compared with traditional organic fluorophores, they offer several advantages including flexible photoexcitation, sharp photoemission as well as superb resistance to photobleaching.^[3–6] Additionally, their optical properties can be tailored to meet specific wavelength requirements by changing the composition or size of

R. Z. Liang, S. M. Xu, D. P. Yan, Dr. W. Y. Shi, R. Tian,
Dr. H. Yan, Prof. M. Wei, Prof. D. G. Evans,
Prof. X. Duan
State Key Laboratory of Chemical Resource Engineering
Beijing University of Chemical Technology
Beijing 100029, P. R. China
E-mail: weimin@mail.buct.edu.cn



DOI: 10.1002/adfm.201201367

polymer/QDs films are not very satisfactory owing to the intertwist of flexible polymer chains, which results in difficulties in controlling homogeneous architecture as well as adjusting their luminescence properties for the multi-color systems. Therefore, to meet the requirements of optical display devices, the development of new materials and strategies for the fabrication of QDs-based systems with ordered superlattice structure and superior photothermal stability is a challenging goal.

So far, the combination of QDs with inorganic matrices is an important approach towards the assembly of QDs-based hybrid films.^[17–19] Among inorganic counterparts, two-dimensional nanosheets as building blocks to assemble with QDs would be favorable to obtain hybrid films with high degree of ordered sequence. Layered double hydroxides (LDHs) are a large class of 2D inorganic materials, which can be described by the general formula $[M^{II}_{1-x}M^{III}_x(OH)_2]z^+A^{n-}_{z/n}\cdot\gamma H_2O$ (M^{II} and M^{III} are divalent and trivalent metals respectively; A^{n-} is the anion).^[20,21] Recently, the delamination of LDHs into single nanosheets which serve as building blocks for the preparation of organic-inorganic functional UTFs have drawn much interest.^[22,23] This motivates us to take the challenge of fabricating LDH/QDs composite UTFs by alternate assembly of positively charged LDH nanosheets with negatively charged QDs, which would exhibit the following advantages: 1) the 2D architecture of LDH/QDs UTFs facilitates the uniform and homogeneous distribution of QDs and suppresses luminescence quenching; 2) the composition and content of QDs can be precisely controlled by adjusting the assembly cycle and sequence, so as to achieve fine tuning of light emission; and 3) the hybrid UTFs own higher photostability and thermostability in comparison with polymer/QDs systems, as a result of the rigid structure of inorganic LDH component.

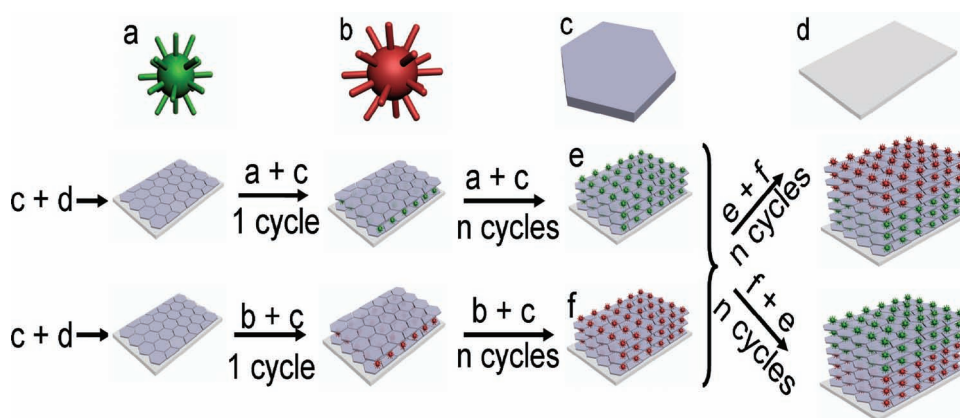
In this work, we report the photoluminescence composite UTFs based on LDH nanosheets and mercaptosuccinic acid modified CdTe QDs, which show highly ordered structure and finely tunable fluorescence. The hybrid UTFs displaying single green or red color luminescence have been fabricated by using two CdTe QDs with different sizes (denoted as CdTe-535 QDs and CdTe-635 QDs; 535 and 635 stand for the luminescence emission peak in aqueous solution, nm); tunable light-emitting

UTFs in the red-green region were subsequently obtained by changing the assembly cycle number and sequence of the two building units. In addition, energy transfer between CdTe-535 QDs and CdTe-635 QDs occurs based on the fluorescence resonance energy transfer (FRET), which extremely enhances the fluorescence intensity of CdTe-635 QDs. Calculation study based on the Förster theory indicates that the FRET between CdTe-535 QDs and CdTe-635 QDs is efficient as the donor-to-acceptor distance r is the double of Förster distance R_0 (R_0 is 6.97 nm). Molecular dynamics (MD) simulations reveal that the CdTe QDs/LDH system exhibits ordered superlattice structure, which is in accordance with the experimental results. Therefore, this work provides a facile approach for the design and fabrication of inorganic-inorganic luminescent UTFs with largely improved behavior, which can serve as promising materials for the integration of multicolor optical and display devices.

2. Results and Discussion

2.1. Fabrication of Red- and Green-Luminescence CdTe QDs/LDH UTFs

Scheme 1 shows the multilayer assembly process of the CdTe QDs/LDH UTFs system. Single green or red UTF was fabricated by alternate deposition of CdTe-535 QDs or CdTe-635 QDs with LDH nanosheets (the detailed information of LDH and CdTe QDs are shown in Figure S1–S6); multiple light-emitting UTFs were obtained by adjusting the cycle number and sequence of the two QDs building units. The $(CdTe-535\ QDs/LDH)_n$ and $(CdTe-635\ QDs/LDH)_n$ ($n = 4–40$) UTFs deposited on quartz substrates were monitored by UV-vis absorption spectroscopy respectively (Supporting Information Figure S7). The intensity of the absorption band at 509 or 614 nm correlates linearly with the bilayer number n , indicative of a stepwise and regular deposition procedure with almost equal amount of CdTe QDs incorporated in each cycle. The density of CdTe-535 QDs and CdTe-635 QDs in a bilayer is $2.46 \times 10^{-3}\ mg/cm^2$ and $2.53 \times 10^{-3}\ mg/cm^2$, respectively. The intensity of the luminescence peak with a maximum at $\sim 541\ nm$ for the



Scheme 1. Schematic representation for the LBL fabrication of multilayer luminous UTFs based on CdTe QDs and LDH nanosheets.

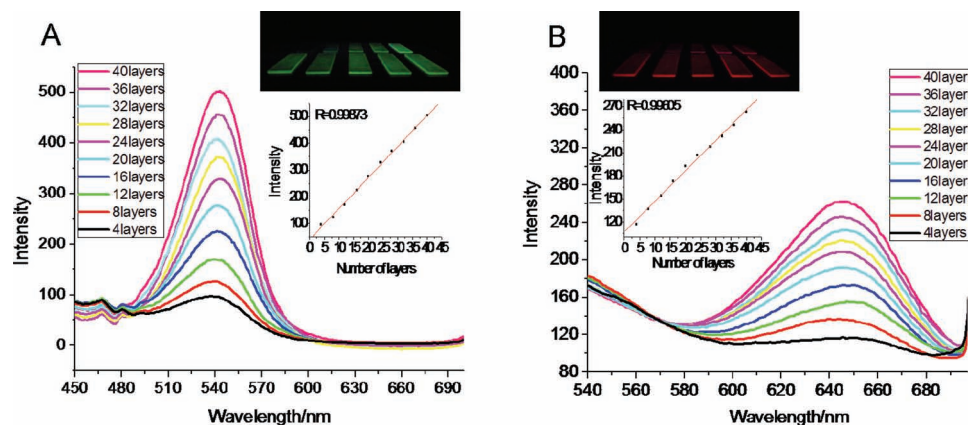


Figure 1. Fluorescence spectra of A) $(\text{CdTe-535 QD/LDH})_n$ UTFs ($n = 4\text{--}40$) and B) $(\text{CdTe-635 QD/LDH})_n$ UTFs ($n = 4\text{--}40$). The inset shows the photographs of these UTFs under UV irradiation.

$(\text{CdTe-535 QDs/LDH})_n$ or ~ 646 nm for the $(\text{CdTe-635 QDs/LDH})_n$ UTFs also displays a monotonic increase along with n (Figure 1). This was further confirmed visually by the gradual increase in the UTFs brightness under ultraviolet irradiation (Figure 1, inset). Photoluminescence quantum yield (PLQY) of the $(\text{CdTe-535 QDs/LDH})_{40}$ and $(\text{CdTe-635 QDs/LDH})_{40}$ UTF is 13.6% and 5.2%, respectively, which was measured by fluorescence spectrometer equipped with an integrating sphere. The luminescence wavelength of the CdTe QDs/LDH UTFs shows a little red-shift compared with the pristine solution of CdTe QDs (Supporting Information Figure S5), which can be ascribed to the interaction between LDH nanosheets and CdTe QDs. In our previous work on the photoluminescence UTFs based on LDHs nanosheets and organic chromophore, it was found that the emitting uniformity can only be maintained within a less bilayer number of building unit (generally below 40 bilayers).^[23] In the case of the CdTe QDs/LDH system however, its fluorescent intensity enhanced gradually along with the increase of deposition cycle and a linear correlation was observed in a broad range up to 80 bilayers (Supporting Information Figure S8). The results indicate that the assembly of LDHs nanosheets with QDs leads to a more superior uniform and ordered structure than that of the LDHs/organic species systems.

2.2. The Structural Characterizations of CdTe QDs/LDH UTFs

The surface morphology and thickness of $(\text{CdTe QDs/LDH})_n$ UTFs were investigated by scanning electron microscopy (SEM). The top view SEM images (Supporting Information Figure S9) display the homogeneity of these UTFs upon increasing bilayer number n , and a typical SEM image for the $(\text{CdTe QDs/LDH})_{40}$ UTFs is shown in Figure 2a,e. The UTFs thickness with various n can be estimated from their side view SEM images (Supporting Information Figure S10; inset of Figure 2a,e). The approximately linear increase of thickness as a function of n was observed, with an average thickness

increment of 4.13 nm and 5.75 nm per bilayer cycle for CdTe-535 QDs/LDH and CdTe-635 QDs/LDH UTFs respectively (Supporting Information Table S1). Small angle XRD patterns of the $(\text{CdTe QDs/LDH})_n$ UTFs show that Bragg diffraction peak is observed at $\sim 2.19^\circ$ for CdTe-535 QDs/LDH and $\sim 1.46^\circ$ for CdTe-635 QDs/LDH (Figure 2b,f; Supporting Information Table S2), accompanied with gradual enhancement in reflection intensity upon increasing bilayer number. This is attributed to a long-range ordered superlattice structure with a periodic repeating distance of 4.03 nm for CdTe-535/LDH UTFs and 6.05 nm for CdTe-635/LDH UTFs respectively, which is approximately consistent with the SEM observations (4.13 and 5.75 nm respectively). The AFM topographical images (2 mm \times 2 mm) of the CdTe QDs/LDH UTFs are illustrated in Figure 2c,g and Supporting Information Figure S11. The value of root-mean-square (rms) roughness for these UTFs increases slowly from 1.50 to 4.28 nm for CdTe-535 QDs/LDH and from 3.51 to 6.27 nm for CdTe-635 QDs/LDH respectively, as the bilayer number varies from 8 to 40 (Supporting Information Table S1), indicating a relatively smooth surface of these UTFs. Furthermore, the $(\text{CdTe-535 QDs/LDH})_{40}$ and $(\text{CdTe-635 QDs/LDH})_{40}$ UTF respectively show homogeneous green and red color with strong brightness under a fluorescence microscope (Figure 2d,h), which indicates that the CdTe QDs are distributed uniformly throughout the UTFs.

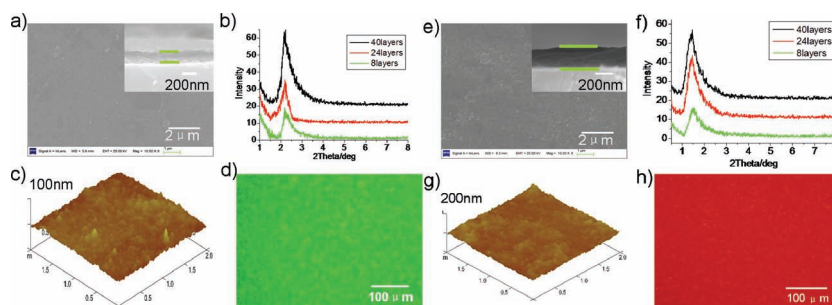


Figure 2. Morphology of the $(\text{CdTe-535 QDs/LDH})_{40}$ and $(\text{CdTe-635 QDs/LDH})_{40}$ UTF: a,e) top-view of SEM images with side-view images shown in the inset; b,f) the small angle XRD patterns; c,g) tapping-mode AFM images; and d,h) fluorescence microscope images.

2.3. Fabrication of CdTe QD/LDH UTFs with Multicolor Light Emission

Our strategy for fabricating multicolor luminescent UTFs involves the stepwise assembly of individual luminescent QDs and LDH nanosheets by changing the QDs type, assembly sequence and bilayer number. We firstly assembled 40 bilayers of CdTe-635 QDs/LDH unit, and continued to assemble the CdTe-535 QDs/LDH unit onto it in order to obtain multiple light-emitting UTFs. UV-vis absorption spectra (Supporting Information Figure S12A) show that the absorbance at ~509 nm increases with n , indicating the gradual growth of CdTe-535 QDs/LDH UTF. The intensity of the fluorescence emission at 541 nm attributed to the CdTe-535 QDs/LDH unit displays a monotonic increase as a function of n (Figure 3a); while the peak at 646 nm attributed to the (CdTe-635 QDs/LDH)₄₀ unit decreases gradually along with the deposition of CdTe-535 QDs/LDH unit. The UTFs color can be tuned from red to

green by increasing the bilayer number of CdTe-535 QDs/LDH unit in the LBL assembly process (Figure 3c). This was further visually observed by the color coordinate measurements, from which the luminescence color of the UTFs changes from red (Supporting Information Table S3, CIE 1931: (0.6710, 0.2892); $n = 0$) to orange (CIE 1931: (0.5108, 0.4167); $n = 10$) and then to yellowgreen (CIE 1931: (0.3372, 0.5769); $n = 35$) by simply increasing the bilayer number of the green emitting unit CdTe-535 QDs/LDH (CIE 1931: (0.2075, 0.6734)) onto the surface of red one (Figure 3e). Subsequently, inverse assembly procedure was carried out by fabricating the CdTe-635 QDs/LDH unit onto the (CdTe-535 QDs/LDH)₄₀ surface so as to get a reverse change in light-emitting color. The assembly process was monitored by UV-vis absorption spectroscopy after each deposition cycle (Supporting Information Figure S12B), from which a gradual increase in the band intensity at ~614 nm attributed to CdTe-635 QDs was observed. In the case of the fluorescence spectra of the (CdTe-535 QD/LDH)₄₀-(CdTe-635 QD/LDH) _{n}

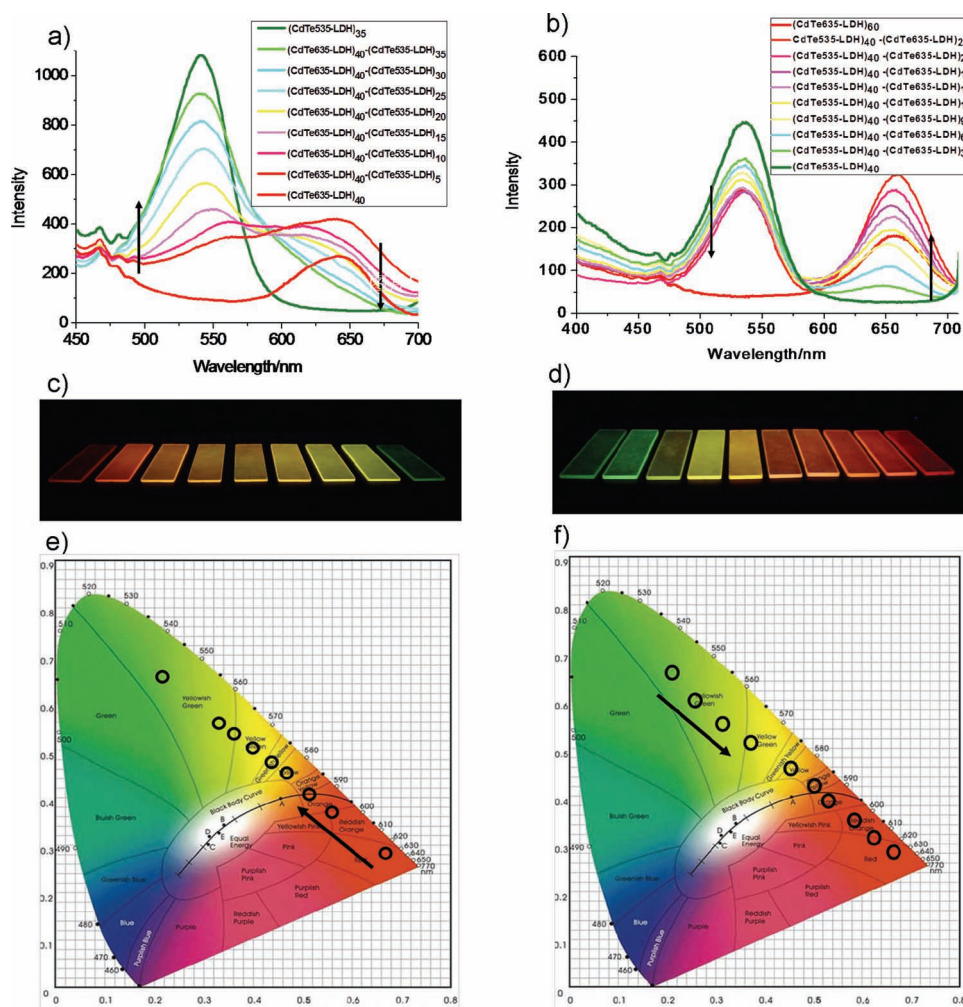


Figure 3. Fluorescence spectra of a) (CdTe-635 QDs/LDH)₄₀-(CdTe-535 QDs/LDH) _{n} UTFs ($n = 5-35$) and b) (CdTe-535 QD/LDH)₄₀-(CdTe-635 QDs/LDH) _{n} UTFs ($n = 3-24$). Photographs of c) (CdTe-635 QDs/LDH)₄₀-(CdTe-535 QDs/LDH) _{n} UTFs and d) (CdTe-535 QD/LDH)₄₀-(CdTe-635 QDs/LDH) _{n} UTFs. The change in color coordinates of e) (CdTe-635 QDs/LDH)₄₀-(CdTe-535 QDs/LDH) _{n} UTFs and f) (CdTe-535 QDs/LDH)₄₀-(CdTe-635 QDs/LDH) _{n} along with the increase of n .

UTFs, the intensity of the sharp peak at ~541 nm displays a consistent decrease while that of 646 nm shows a gradual increase along with n (Figure 3b). It should be noted that the fluorescent intensity at 646 nm for the (CdTe-535 QDs/LDH)₄₀-(CdTe-635 QDs/LDH)₂₄ UTF is nearly two times as (CdTe-635 QDs/LDH)₆₀ UTF. This is probably attributed to the energy transfer from CdTe-535 QDs/LDH unit to CdTe-635 QDs/LDH one, which will be further discussed in the next section. The change in luminescence color under UV irradiation along with the deposition of CdTe-635 QDs/LDH unit is displayed in Figure 3d: the color of the UTFs varies from green (CdTe-535 QDs/LDH)₄₀ (CIE 1931: (0.2075, 0.6734)) to yellow green (CIE 1931: (0.3142, 0.5662); $n = 6$) and then to orange red (CIE 1931: (0.5891, 0.3647); $n = 21$) by simply increasing the bilayer number of CdTe-635 QDs/LDH unit (CIE 1931: (0.6710, 0.2892)) (see Figure 3f and Supporting Information Table S4). Therefore, a precise tuning of the luminescent emission of the UTFs in the red-green region can be achieved via adjusting the assembly sequence and bilayer number.

2.4. Energy Transfer between CdTe-535 and CdTe-635 QDs

In order to confirm whether the energy transfer occurs or not, the assembly number and sequence of the CdTe-535 QDs/LDH and CdTe-635 QDs/LDH unit were adjusted (Figure 4). Curve a and b in Figure 4A represent the (CdTe-535 QDs/LDH)₅ and (CdTe-635 QDs/LDH)₅ UTF with single building unit respectively, and curve c displays the ((CdTe-535 QDs/LDH)@(CdTe-635 QDs/LDH))₅ UTF by alternate assembly with the two units for 5 cycles. The former two UTFs show a strong emission peak at 541 nm and a rather weak one at 646 nm respectively; whereas the latter UTF shows a much decreased emission at 541 nm and a largely enhanced one at 646 nm. This indicates an energy transfer from the CdTe-535 QDs/LDH unit to the CdTe-635 QDs/LDH one. Time-resolved emission spectroscopy further provides a direct evidence for FRET (Figure 4C). The fluorescence intensity at 541 nm decays gradually while the intensity at 646 nm increases firstly to a maximum and then decreases in the whole excitation time. This indicates the occurrence of FRET from CdTe-535 QDs to CdTe-635 QDs, accounting for the original enhancement at the low-energy emission (646 nm). Based on the PL quenching of the (CdTe-535 QDs/LDH)₅ unit, the FRET efficiency (E) in the hybrid UTF was estimated to be 56% according to $E = 1 - F_{DA}/F_D$, where F_{DA} is the integrated fluorescence intensity of donor in the presence of acceptor and F_D is the integrated fluorescence intensity of

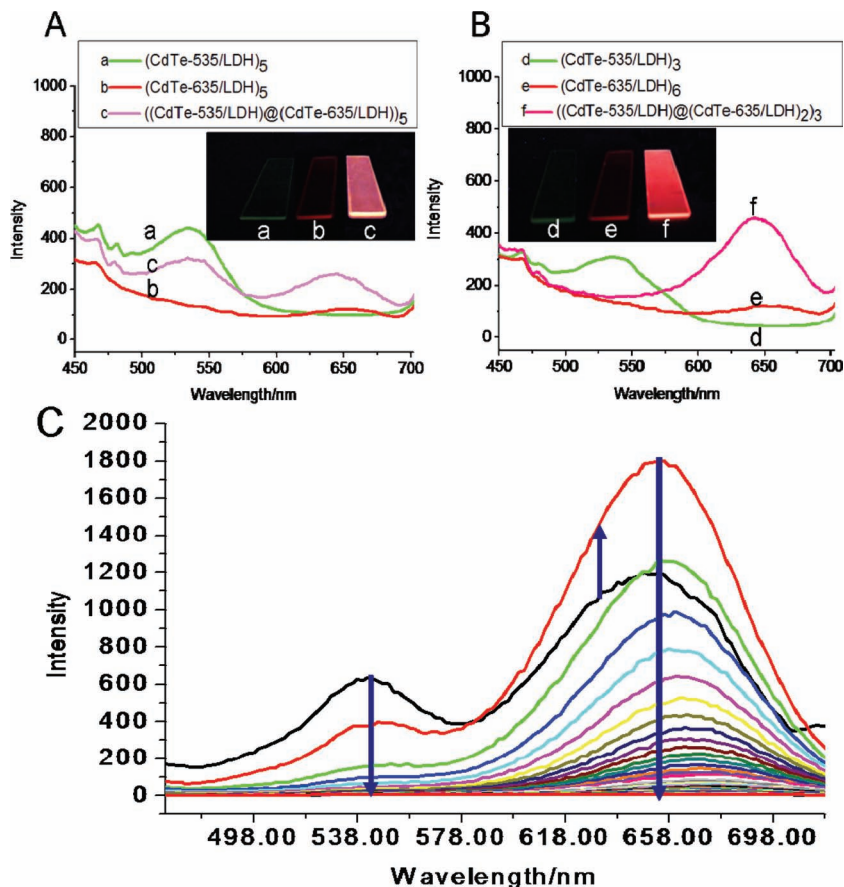


Figure 4. A) Fluorescence spectra of a) (CdTe-535 QDs/LDH)₅, b) (CdTe-635 QDs/LDH)₅, and c) ((CdTe-535 QDs/LDH)@(CdTe-635 QDs/LDH))₅ UTF. B) Fluorescence spectra of d) (CdTe-535 QDs/LDH)₃, e) (CdTe-635 QDs/LDH)₆, and f) ((CdTe-535 QDs/LDH)@(CdTe-635 QDs/LDH)₂)₃ UTF. The inset shows the photographs of these samples. C) Time-resolved emission spectroscopy of the ((CdTe-535 QDs/LDH)@(CdTe-635 QDs/LDH))₅ UTF.

donor alone (no acceptor present).^[24] We also changed the composition of repeating unit so as to obtain a higher FRET efficiency. Curve d and e in Figure 4B exhibit the (CdTe-535 QDs/LDH)₃ and (CdTe-635 QDs/LDH)₆ UTF respectively, while curve f shows the ((CdTe-535 QDs/LDH)@(CdTe-635 QDs/LDH)₂)₃ UTF by assembling the repeating unit of (CdTe-535 QDs/LDH)@(CdTe-635 QDs/LDH)₂ for 3 cycles. It can be observed that curve d and e display a weak emission at 541 and 646 nm respectively; however, the hybrid UTF (curve f) shows a much stronger peak at 646 nm with the absence of emission at 541 nm. A higher FRET efficiency of 91% was obtained in this case, indicating that the energy transfer occurs more sufficiently in the (CdTe-535 QDs/LDH)@(CdTe-635 QDs/LDH)₂ unit than the (CdTe-535 QDs/LDH)@(CdTe-635 QDs/LDH) one. As a result, the fluorescent intensity of red emission can be immensely promoted by adjusting the assembly number and sequence of the two QDs building units. It was reported that the Förster distance in a FRET system plays a key role in determining its FRET efficiency,^[24] and this will be further discussed in the computational section below.

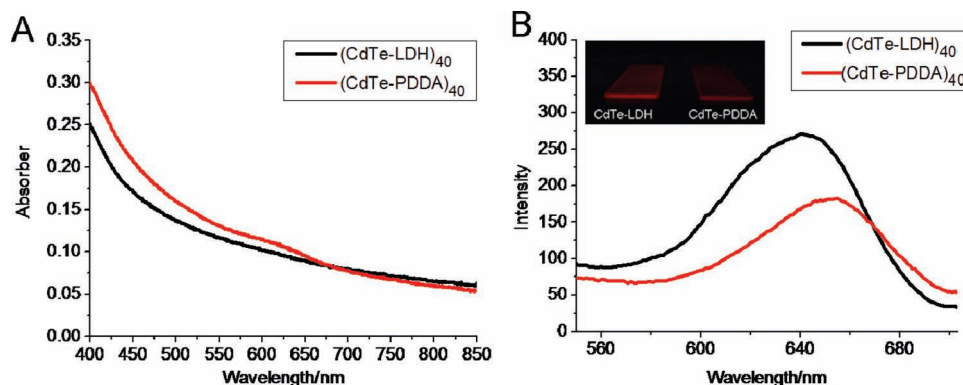


Figure 5. A) UV-vis absorption spectra and B) fluorescence spectra of the (CdTe-635 QDs/LDH)₄₀ UTF and (CdTe-635 QDs/PDDA)₄₀ UTF.

2.5. A Comparison of CdTe QDs/LDH UTF and CdTe QDs/PDDA UTF

It is instructive to further compare the photophysical properties of CdTe QDs/LDH with other CdTe QDs/polymer systems. PDDA was chosen as the polycation to alternatively assemble with CdTe QDs. The (CdTe-635 QDs/LDH)₄₀ UTF displays a close absorbance at 614 nm to that of the (CdTe-635 QDs/PDDA)₄₀ UTF (Figure 5A), indicating a close content of CdTe-635 QDs involved in the two composite UTFs. However, the (CdTe-635 QDs/LDH)₄₀ UTF exhibits a much stronger fluorescence emission than the (CdTe-635 QDs/PDDA)₄₀ one (Figure 5B). In addition, an obvious red shift for the (CdTe-635 QDs/PDDA)₄₀ UTF was observed compared with the (CdTe-635 QDs/LDH)₄₀ UTF, possibly resulting from a more serious aggregation of CdTe-635 QDs in PDDA matrix than in LDH one. This also accounts for the lower fluorescence intensity of the (CdTe-635 QDs/PDDA)₄₀ UTF in comparison with the (CdTe-635 QDs/LDH)₄₀ one. The small angle XRD pattern of the (CdTe-635 QDs/LDH)₄₀ shows a rather strong reflection at 2θ 1.46° while a weak one at 2θ 1.12° was observed for the (CdTe-635 QDs/PDDA)₄₀ UTF (Figure 2f, Supporting Information Figure S13A), indicating a more ordered superlattice structure of the (CdTe-635 QDs/LDH)₄₀ UTF. Moreover, the RSM roughness of AFM image for the (CdTe-635 QDs/LDH)₄₀ UTF is 6.27 nm, much lower than that of the (CdTe-635 QDs/

PDDA)₄₀ one (14.62 nm, Supporting Information Figure S13B). The results above show that the CdTe-635 QDs/LDH UTF possesses higher degree of stacking order and uniformity than the CdTe-635 QDs/PDDA system, as a result of the highly ordered 2D architecture fabricated by the LDH nanosheets and CdTe QDs.

Photo- and thermostability are extremely important criteria in practical applications of photonic or optoelectronic devices. The fluorescence intensities of CdTe-635 QDs/PDDA and CdTe-635 QDs/LDH UTF were recorded by illuminating them with UV light in a comparative study. After a 5 h irradiation, the fluorescent intensity of the CdTe-635 QDs/PDDA UTF decreased 49% while only 26% loss was found for the CdTe-635 QDs/LDH UTF (Figure 6A). This verifies that the CdTe QDs/LDH system possesses a better UV-resistance stability than the CdTe QDs/PDDA one. The reason for better photo and thermal stability of the LDH-CdTe film relative to the PDDA-CdTe film is that the configurational change of organic polymer under UV light irradiation would result in the aggregation of QDs; while the LDH nanosheets provide a rigid and confined 2D microenvironment for the ordered and uniform dispersion of QDs, which suppresses their migration/aggregation under UV irradiation. Both the CdTe-635 QDs/PDDA and CdTe-635 QDs/LDH UTF undergo a decrease in luminescence intensity upon heating at 80 °C for 2 min (Figure 6B). For the CdTe-635 QDs/PDDA UTF, the intensity sharply decreased to 47% of its

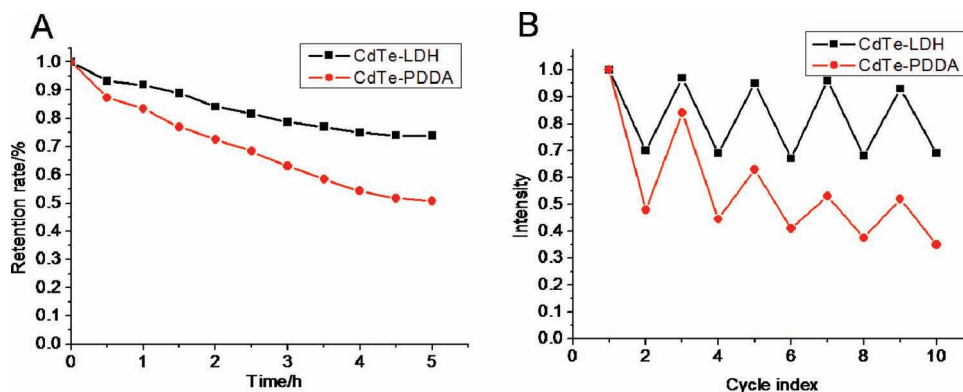


Figure 6. A) Photostability and B) thermostability of the (CdTe-635 QDs/LDH)₄₀ and (CdTe-635 QDs/PDDA)₄₀ UTF.

original value, and only recovered to 83% after the UTF was cooled to 20 °C. Continuous decrease in luminescence emission was observed in the following heating-cooling cycles. In contrast, the intensity of the CdTe-635 QDs/LDH UTF diminished to 70% of its original value being heated to 80 °C and almost recovered to its original intensity after cooling; this cycle can be performed for several times without significant emission loss. Generally, the geometrical or electronic structure of organic polymer changes easily under thermal agitation and gives rise to spontaneous transformation of fluorescence,^[17] leading to fluorescence quenching of the CdTe-635 QDs/PDDA UTF. As a comparison, the QDs are confined between the rigid LDH nanosheets and thus become insensitive to thermal relaxation. Therefore, the decrease in luminescence intensity of the CdTe-635 QDs/LDH UTF can be attributed to escalated interaction between exciton and longitudinal optical phonon in the CdTe core at elevated temperature, resulting in enhanced non-radiative decay.^[25]

2.6. Theoretical Study on the CdTe QDs/LDH and CdTe QDs/PDDA System

In order to further intuitively understand the energy transfer between the two CdTe QDs, the theory of Förster^[26] was employed to estimate the FRET efficiency (E) occurring in single donor (CdTe-535 QDs) and single acceptor (CdTe-635 QDs). E is given by:

$$E = \frac{R_0^6}{R_0^6 + r^6} \quad (1)$$

where r is the distance between donor and acceptor; R_0 is the Förster distance which represents the donor-to-acceptor distance (r) as FRET efficiency is 50%. R_0 was calculated to be 6.97 nm in this work (see calculation details in the Supporting Information), and the relationship between E and r is shown in Supporting Information Figure S14, from which it is concluded that FRET can occur as r is within 13.94 nm. Based on the XRD pattern, the closest donor-to-acceptor distance in the CdTe-535 QDs/LDH@CdTe-635 QDs/LDH unit is ~5 nm, while it is ~11 nm for CdTe-535 QDs and CdTe-635 QDs of the second layer in the (CdTe-535 QDs/LDH)@(CdTe-635 QDs/LDH)₂ unit. Therefore, the latter repeating unit shows a higher FRET efficiency than the former one. The results also match well with the experimental findings that the FRET efficiency of ((CdTe-635 QDs/LDH)@(CdTe-635 QDs/LDH))₃ UTF exceeds 90% whereas only 56% is observed for the ((CdTe-635 QDs/LDH)@(CdTe-635 QDs/LDH))₅ UTF (Figure 4).

In addition, molecular dynamics (MD) simulations were performed on the CdTe QDs/LDH system in comparison with CdTe QDs/PDDA one to shed light on the configuration and distribution of the CdTe QDs in these two matrices. Four models were constructed to represent CdTe-535 QDs/LDH, CdTe-635 QDs/LDH, CdTe-535 QDs/PDDA and CdTe-635 QDs/PDDA respectively, whose formulae are listed in Supporting Information Table S5. The side view and top view of these four systems at $t = 0$ ps are displayed in Figure 7a–d and Supporting Information Figure S15, respectively. Computational details are described in the Supporting Information.

As shown in Supporting Information Figure S16, each system can attain equilibration within 30 ps. Figure 7e,f and Supporting Information Figure S17 illustrate the side view and

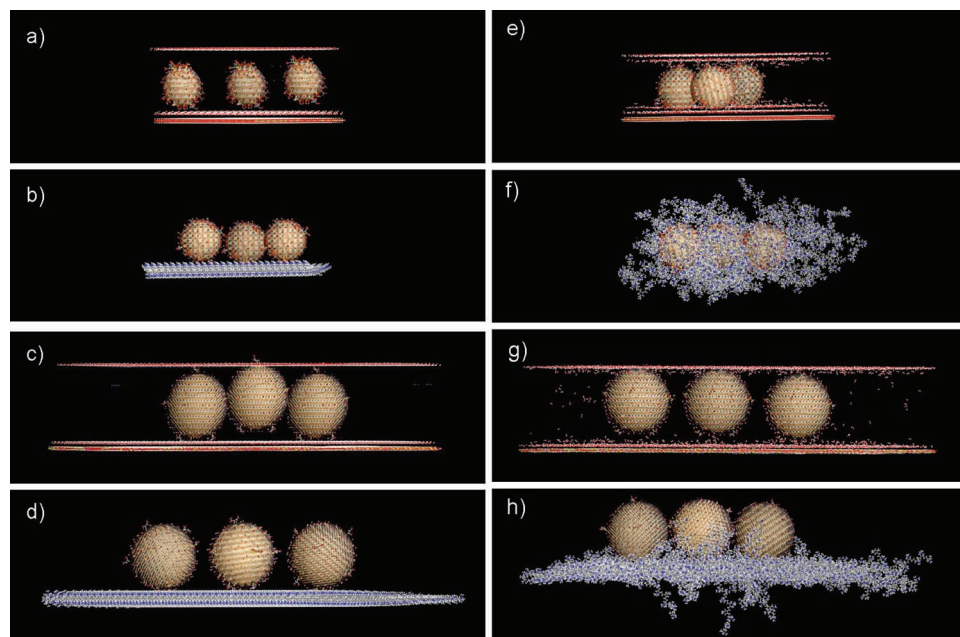


Figure 7. Side view at $t = 0$ ps for a) CdTe-535 QDs/LDH, b) CdTe-535 QDs/PDDA, c) CdTe-635 QDs/LDH, and d) CdTe-635 QDs/PDDA. Side view at $t = 30$ ps for e) CdTe-535 QDs/LDH, f) CdTe-535 QDs/PDDA, h) CdTe-635 QDs/LDH, and g) CdTe-635 QDs/PDDA. The color denotation: green for Mg, pink for Al, red for O, white for H, silver white for Cd, orange for Te, grey for C, blue for N, yellow for S, purple for Na (see Supporting Information Figure S22 for more information).

top view of these four systems at $t = 30$ ps, from which a more ordered structure as well as smooth surface are observed for the CdTe QDs/LDH system than those of the CdTe QDs/PDDA one. The side view and top view of these four systems at $t = 15$ ps are also displayed in Supporting Information Figure S18 and Supporting Information Figure S19, indicating the process of dynamic changes. The interlayer spacings of CdTe-535 QDs/LDH and CdTe-635 QDs/LDH are 4.02 nm and 5.66 nm respectively (Supporting Information Table S6), which agrees well with 4.03 nm and 6.05 nm obtained by small angle XRD (Figure 2). Moreover, the layered structure can be well maintained for CdTe QDs/LDH while intertwist was found in the CdTe QDs/PDDA system at equilibration. Furthermore, the distance distribution of two adjacent QDs in the CdTe QDs/LDH system was recorded every 100 fs during the next 30 ps after equilibration (Supporting Information Figure S20 and S21), which varies in a very narrow range (~ 0.6 nm). This indicates that the mobility of QDs is seriously restricted in the LDH gallery. However, the movement of QDs can not be suppressed in the absence of effective confinement in the PDDA matrix, as a result the distance distribution of two adjacent QDs in one layer was not obtained. Therefore, both the experimental and theoretical study prove that the CdTe QDs/LDH system owns a more ordered and homogeneous 2D layered architecture, which results in its higher stability and stronger fluorescence emission than the CdTe QDs/PDDA one.

3. Conclusions

In conclusion, a feasible LBL strategy was developed for the fabrication of single-color and multicolor luminescent UTFs based on the combination of anionic CdTe QDs and positively charged LDH nanosheets. The luminescence color of the resulting hybrid UTFs can be easily tuned over the whole red-green region by changing the QDs size, assembly sequence and deposition cycle number. The UTFs exhibit a periodic long-range stacking order structure, uniform morphology and controllable thickness on the nanometer scale. Energy transfer between CdTe-535 QDs/LDH and CdTe-635 QDs/LDH can extremely enhance the fluorescence intensity of the CdTe-635 QDs/LDH unit and the resulting multiple light-emitting UTFs. Furthermore, the UTFs based on the incorporation of CdTe QDs and LDH nanosheets possess stronger fluorescent intensity, higher photostability and thermostability compared with those of CdTe QDs/polyelectrolyte system. Therefore, this work provides a highly ordered luminescent UTFs fabricated by distributing QDs within an inorganic 2D nanosheets matrix, which would facilitate both fundamental understanding and technological applications in biological sensors, photonic and multicolor photoemission devices.

4. Experimental Section

Chemicals: Polydimethylallylammonium chloride (PDDA, $M_w = 100\,000$ – $200\,000$), $Al_2(Te)_3$, $Cd(ClO_4)_2 \cdot 6H_2O$, mercaptosuccinic acid were purchased from Sigma Chemical. Co. Ltd. Analytical pure $Mg(NO_3)_2 \cdot 6H_2O$, $Al(NO_3)_3 \cdot 9H_2O$, NaOH, C_2H_5OH , H_2SO_4 and urea were used without further purification. The deionized and decarbonated water was used in all the experimental processes.

Synthesis of MgAl- NO_3 -LDH Nanosheets: The process of synthesis and exfoliation of MgAl- NO_3 -LDH was similar to that described in our previous work.^[27] Typically, $Mg(NO_3)_2 \cdot 6H_2O$ (0.002 mol), $Al(NO_3)_3 \cdot 9H_2O$ (0.001 mol) and urea (0.012 mol) were dissolved in aqueous solution (70 cm^3). The mixture was sealed in a teflon-lined stainless steel autoclave and heated at 100 °C for 24 h. The material was washed with water and dried in air at 60 °C. The transformation from MgAl- CO_3 -LDH to MgAl- NO_3 -LDH was achieved by the following method: a sample of MgAl- CO_3 -LDH (0.3 g) was treated with 300 cm^3 of an aqueous solution containing $NaNO_3$ (0.50 mol) and HNO_3 (0.0015 mol) whilst purging with nitrogen gas, and was shaken for 1 day at ambient temperature (25 °C). The resulting MgAl- NO_3 -LDH was washed with hot distilled water, and then dried in a vacuum at 60 °C. 0.1 g of this sample was shaken in 100 cm^3 of formamide solution for 24 h to produce a colloidal suspension of exfoliated MgAl-LDH nanosheets.

Preparation of CdTe QDs: The aqueous synthesis of mercaptosuccinic acid modified CdTe QDs was referred to the reported method.^[28] In a typical synthesis, 0.985 g (2.35 mmol) of $Cd(ClO_4)_2 \cdot 6H_2O$ was dissolved in water (125 mL); 0.278 g of mercaptosuccinic acid stabilizer was added under stirring, followed by adjusting the pH value to be 11 with addition of a NaOH solution (1.0 M). The solution was placed in a three-necked flask fitted with a septum valves and was deaerated by N_2 bubbling for 30 min. Under stirring, H_2Te gas generated by $Al_2(Te)_3$ and H_2SO_4 was purged into the solution together with a slow nitrogen flow, and CdTe QD precursor was formed at this stage. The formation and growth of QDs proceed upon refluxing at 100 °C under open-air conditions with an attached condenser. The fluorescent color of CdTe QDs solution changes from green to red upon increasing refluxing time. The refluxing time for CdTe-535 QDs and CdTe-635 QDs was 10 min and 2 h, respectively.

Assembly of CdTe QDs/LDH UTFs: The quartz glass substrate was first cleaned in concentrated $NH_3/30\% H_2O_2$ (7:3) and concentrated H_2SO_4 for 30 min each, and then was washed thoroughly with deionized water. The substrate was dipped into a colloidal suspension of MgAl-LDH nanosheets (1.0 $g\ dm^{-3}$) for 10 min followed by washing thoroughly, and then was treated with CdTe QDs aqueous solution (0.15 $g\ dm^{-3}$) for another 10 min. Multilayer UTFs of $(CdTe\ QDs/LDH)_n$ were fabricated by repeating the above deposition process for n cycles. The resulting UTFs were dried with a nitrogen gas flow for 2 min at 25 °C. The $(CdTe\ QDs/PDDA)_n$ UTFs were prepared with a similar LBL method to that of $(CdTe\ QDs/LDH)_n$. The concentration of PDDA and CdTe QDs were 1.0 $g\ dm^{-3}$ and 0.15 $g\ dm^{-3}$, respectively.

Techniques of Characterization: The solid UV-vis absorption spectra were collected in the range from 400 to 850 nm on a Shimadzu U-3000 spectrophotometer, with the slit width of 1.0 nm. The fluorescence spectra were performed on a RF-5301PC fluorospectrophotometer with the excitation wavelength of 360 nm. The fluorescence emission spectra are in the range from 450 to 700 nm, and the width of both the excitation and emission slit is 3 nm for CdTe QDs-535/LDH UTFs and 5 nm for CdTe QDs-635/LDH UTFs respectively. The color coordinates of the fluorescence were determined by a PR-650 spectroradiometer. XRD patterns of CdTe QDs/LDH UTFs were recorded using a Rigaku 2500VB2+PC diffractometer under the conditions: 40 kV, 50 mA, Cu $K\alpha$ radiation with step-scanned in step of 0.04° (2θ) in the range from 0.5 to 8° using a count time of 10 s/step. The morphology of UTFs was investigated by using a scanning electron microscope (SEM Hitachi S-3500) equipped with an EDX attachment (EDX Oxford Instrument Isis 300), and the accelerating voltage applied was 20 kV. The surface roughness data were obtained by using a NanoScope IIIa atomic force microscope (AFM) from Veeco Instruments. TEM images were recorded on a JEOL JEM-2100 transmission electron microscope with the accelerating voltage of 200 kV. Fluorescence was observed using an OLYMPUS-BX51 fluorescence microscope. The photobleaching was tested by the UV lighting with CHF-XQ 500W. Photoluminescence quantum yield was measured using a Nanolog FL3-2iHR infrared fluorescence spectrometer equipped with an integrating sphere. Time-resolved emission spectra were recorded by a LifeSpec Red Spectrometer.

Supporting Information

Supporting Information is available from the Wiley Online Library or from the author.

Acknowledgements

This project was supported by the National Natural Science Foundation of China, the 973 Program (Grant No.: 2011CBA00504), the 111 Project (Grant No. B07004) and the Collaboration Project from the Beijing Education Committee.

Received: May 21, 2012

Published online: July 20, 2012

- [1] a) C. Burda, X. Chen, R. Narayanan, M. A. El-Sayed, *Chem. Rev.* **2005**, *105*, 1025; b) J. M. Bruchez, M. Moronne, P. Gin, S. Weiss, A. P. Alivisatos, *Science* **1998**, *281*, 2013; c) V. I. Klimov, A. A. Mikhailovsky, S. Xu, A. Malko, J. A. Hollingsworth, C. A. Leatherdale, H. J. Eisler, M. G. Bawendi, *Science* **2000**, *290*, 314; d) V. I. Klimov, S. A. Ivanov, J. Nanda, M. Achermann, I. Bezel, J. A. McGuire, A. Piryatinski, *Nature* **2007**, *447*, 441.
- [2] a) Q. J. Sun, G. Subramanyam, L. M. Dai, M. Check, A. Campbell, R. Naik, J. Grote, Y. Q. Wang, *ACS Nano* **2009**, *3*, 737; b) M. Lee, R. S. Yang, C. Li, Z. L. Wang, *J. Phys. Chem. Lett.* **2010**, *1*, 2929; c) F. Todescato, I. Fortunati, S. Gardin, E. Garbin, E. Collini, R. Bozio, J. J. Jasieniak, G. D. Giustina, G. Brusatin, S. Toffanin, R. Signorini, *Adv. Funct. Mater.* **2012**, *22*, 337; d) S. De, A. Layek, A. Raja, A. Kadir, M. R. Gokhale, A. Bhattacharya, S. Dhar, A. Chowdhury, *Adv. Funct. Mater.* **2011**, *21*, 3828.
- [3] X. Gao, L. Yang, J. A. Petros, F. F. Marshall, J. W. Simons, S. Nie, *Curr. Opin. Biotechnol.* **2005**, *16*, 63.
- [4] a) F. Fleischhaker, R. Zentel, *Chem. Mater.* **2005**, *17*, 1346; b) P. Peumans, A. Yakimov, S. R. Forrest, *J. Appl. Phys.* **2003**, *93*, 3693.
- [5] a) T. Baron, A. Fernandes, J. F. Damlencourt, B. De Salvo, F. Martin, F. Mazen, S. Haukka, *Appl. Phys. Lett.* **2003**, *82*, 4151; b) A. H. Mueller, M. A. Petruska, M. Achermann, D. J. Werder, E. A. Akhador, D. D. Koleske, M. A. Hoffbauer, V. I. Klimov, *Nano Lett.* **2005**, *5*, 1039.
- [6] a) H. Mattoussi, J. M. Mauro, E. R. Goldman, G. P. Anderson, V. C. Sundar, F. V. Mikulec, M. G. Bawendi, *J. Am. Chem. Soc.* **2000**, *122*, 12142; b) E. R. Goldman, G. P. Anderson, P. T. Tran, H. Mattoussi, P. T. Charles, J. M. Mauro, *Anal. Chem.* **2002**, *74*, 841.
- [7] A. P. Alivisatos, *Science* **1996**, *271*, 933.
- [8] a) O. Kulakovich, N. Strekal, A. Yaroshevich, S. Maskevich, S. Gaponenko, I. Nabiev, U. Woggon, M. Artemyev, *Nano Lett.* **2002**, *2*, 1449; b) Y. Guo, D. L. Shi, H. Cho, Z. Y. Dong, A. Kulkarni, G. M. Pualetti, W. Wang, J. Lian, W. Liu, L. Ren, Q. Q. Zhang, G. K. Liu, C. Huth, L. M. Wang, R. C. Ewing, *Adv. Funct. Mater.* **2008**, *18*, 2489; c) B. Atmaja, B. H. Lui, Y. Hu, S. E. Beck, C. W. Frank, J. R. Cochran, *Adv. Funct. Mater.* **2010**, *20*, 4091; d) S. Laurent, D. Forge, M. Port, A. Roch, C. Robic, L. V. Elst, R. N. Muller, *Chem. Rev.* **2008**, *108*, 2064.
- [9] D. V. Talapin, J. S. Lee, M. V. Kovalenko, E. V. Shevchenko, *Chem. Rev.* **2010**, *110*, 389.
- [10] a) J. Zhao, J. Zhang, C. Jiang, J. Bohnenberger, T. Basché, A. Mews, *J. Appl. Phys.* **2004**, *96*, 3206; b) S. Coe, W. K. Woo, M. Bawendi, V. Bulovic, *Nature* **2002**, *420*, 800.
- [11] A. A. Mamedov, A. Belov, M. Giersig, N. N. Mamedova, N. A. Kotov, *J. Am. Chem. Soc.* **2001**, *123*, 7738.
- [12] S. Jaffar, K. T. Nam, A. Khademhosseini, J. Xing, R. S. Langer, A. M. Belcher, *Nano Lett.* **2004**, *4*, 1421.
- [13] Y. Wang, Z. Tang, M. A. Correa-Duarte, L. M. Liz-Marzán, N. A. Kotov, *J. Am. Chem. Soc.* **2003**, *125*, 2830.
- [14] Y. W. Lin, W. L. Tseng, H. T. Chang, *Adv. Mater.* **2006**, *18*, 1381.
- [15] W. K. Bae, J. Kwak, J. Lim, D. Lee, M. K. Nam, K. Char, C. Lee, S. Lee, *Nano Lett.* **2010**, *10*, 2368.
- [16] D. P. Yan, J. Lu, M. Wei, S. H. Qin, L. Chen, S. T. Zhang, D. G. Evans, X. Duan, *Adv. Funct. Mater.* **2011**, *21*, 2497.
- [17] B. Qin, H. Y. Chenname, H. Liang, L. Fu, X. F. Liu, X. H. Qiu, S. Q. Liu, R. Song, Z. Y. Tang, *J. Am. Chem. Soc.* **2010**, *132*, 2886.
- [18] a) J. M. Caruge, J. E. Halpert, V. Wood, V. Bulovic, M. G. Bawendi, *Nat. Photonics* **2008**, *2*, 247; b) T. Franzl, T. A. Klar, S. Schietinger, A. L. Rogach, J. Feldmann, *Nano Lett.* **2004**, *4*, 1599; c) T. Kameyama, K. Okazaki, Y. Ichikawa, A. Kudo, S. Kuwabata, T. Torimoto, *Chem. Lett.* **2008**, *37*, 700.
- [19] a) J. S. Bendall, M. Paderi, F. Ghigliotti, N. L. Pira, V. Lambertini, V. Lesnyak, N. Gaponik, G. Visimberga, A. Eychmüller, C. M. S. Torres, M. E. Welland, C. Gieck, L. Marchese, *Adv. Funct. Mater.* **2010**, *20*, 3298; b) T. Kameyama, K. Okazaki, K. Takagia, T. Torimoto, *Phys. Chem. Chem. Phys.* **2009**, *11*, 5369.
- [20] a) A. I. Khan, L. X. Lei, A. J. Norquist, D. O'Hare, *Chem. Commun.* **2001**, 2342; b) L. F. S. Silva, G. J. F. Demets, C. T. Guého, F. Leroux, J. B. Valim, *Chem. Mater.* **2011**, *23*, 1350; c) A. M. Fogg, A. J. Freij, G. M. Parkinson, *Chem. Mater.* **2002**, *14*, 232; d) G. M. Lombardo, G. C. Pappalardo, F. Costantino, U. Costantino, M. Sisani, *Chem. Mater.* **2008**, *20*, 5585.
- [21] a) A. M. Fogg, V. M. Green, H. G. Harvey, D. O'Hare, *Adv. Mater.* **1999**, *11*, 1466; b) A. M. Fogg, J. S. Dunn, S. G. Shyu, D. R. Cary, D. O'Hare, *Chem. Mater.* **1998**, *10*, 351; c) U. Costantino, M. Nocchetti, R. Vivani, *J. Am. Chem. Soc.* **2002**, *124*, 8428; d) F. Leroux, J. P. Besse, *Chem. Mater.* **2001**, *13*, 10.
- [22] a) Z. P. Liu, R. Z. Ma, M. Osada, N. Iyi, Y. Ebina, K. Takada, T. Sasaki, *J. Am. Chem. Soc.* **2006**, *128*, 4872; b) J. H. Lee, J. Chang, J. H. Cha, D. Y. Jung, S. S. Kim, J. M. Kim, *Chem. Eur. J.* **2010**, *16*, 8296; c) J. B. Han, D. P. Yan, W. Y. Shi, J. Ma, H. Yan, M. Wei, G. D. Evans, X. Duan, *J. Phys. Chem. B* **2010**, *114*, 5678.
- [23] a) D. P. Yan, J. Lu, M. Wei, J. Ma, D. G. Evans, X. Duan, *Chem. Commun.* **2009**, 6358; b) W. Y. Shi, Y. J. Lin, X. G. Kong, S. T. Zhang, Y. K. Jia, M. Wei, D. G. Evans, X. Duan, *J. Mater. Chem.* **2011**, *21*, 6088.
- [24] a) A. R. Clapp, I. L. Medintz, J. M. Mauro, B. R. Fisher, M. G. Bawendi, H. Mattoussi, *J. Am. Chem. Soc.* **2004**, *126*, 301; b) P. T. K. Chin, R. A. M. Hikmet, S. C. J. Meskers, R. A. J. Janssen, *Adv. Funct. Mater.* **2007**, *17*, 3829.
- [25] S. Li, K. Zhang, J. M. Yang, L. W. Lin, H. Yang, *Nano Lett.* **2007**, *7*, 10.
- [26] J. R. Lakowicz, *Principles of Fluorescence Spectroscopy*, Kluwer Academic, New York **1999**.
- [27] D. P. Yan, J. Lu, M. Wei, J. B. Han, J. Ma, F. Li, D. G. Evans, X. Duan, *Angew. Chem. Int. Ed.* **2009**, *48*, 3073.
- [28] N. P. Gaponik, D. V. Talapin, A. L. Rogach, K. Hoppe, E. V. Shevchenko, A. Kornowski, A. Eychmüller, H. Weller, *J. Phys. Chem. B* **2002**, *106*, 7177.